Experiments and simulations on short chain fatty acid production in a colonic bacterial community

Bea Yu,[a] Ilija Dukovski,[b,c] David Kong,[d] Johanna Bobrow,[a] Alla Ostrinskaya,[a] Daniel Segrè[b,c,e]#, Todd Thorsen [a]#

[a]MIT Lincoln Lab, 244 Wood Street, Lexington, MA 02421, USA

[b]Bioinformatics Graduate Program, Boston University, Boston, MA 02215, USA [c]Biological Design Center, Boston University, Boston, MA 02215, USA

[d]Director, Community Biotechnology Initiative, MIT Media Lab, Massachusetts Institute of Technology, 77 Mass. Ave., E14/E15, Cambridge, MA 02139 USA

[e]Department of Biology, Department of Biomedical Engineering and Department of Physics, Boston University, Boston, MA 02215, USA

Running Head: Study of *F. prausnitzii-B. thetaiotaomicron* coculture

#Address correspondence to: Daniel Segrè, dsegre@bu.edu and Todd Thorsen, thorsen@ll.mit.edu

B.Y. and I.D. contributed equally to this work.

DISTRIBUTION STATEMENT A. Approved for public release. Distribution is unlimited.

This material is based upon work supported by the Assistant Secretary of Defense for Research and Engineering under Air Force Contract No. FA8702-15-D-0001. Any opinions, findings, conclusions or recommendations expressed in this material are those of the author(s) and do not necessarily reflect the views of the Assistant Secretary of Defense for Research and Engineering.

Abstract

Understanding how production of specific metabolites by gut microbes is modulated by interactions with surrounding species and by environmental nutrient availability is an important open challenge in microbiome research. As part of this endeavor, this work explores interactions between *F. prausnitzii,* a major butyrate producer, and *B. thetaiotaomicron*, an acetate producer, under three different *in vitro* media conditions in monoculture and coculture. *In silico* Genome-scale dynamic flux balance analysis (dFBA) models of metabolism in the system using COMETS (Computation of Microbial Ecosystems in Time and Space) are also tested for explanatory, predictive and inferential power. Experimental findings indicate enhancement of butyrate production in coculture relative to *F. prausnitzii* monoculture but defy a simple model of monotonic increases in butyrate production as a function of acetate availability in the medium. Simulations recapitulate biomass production curves for monocultures and accurately predict the growth curve of coculture total biomass, using parameters learned from monocultures, suggesting that the model captures some aspects of how the two bacteria interact. However, a comparison of data and simulations for environmental acetate and butyrate changes suggest that the organisms adopt one of many possible metabolic strategies equivalent in terms of growth efficiency. Furthermore, the model seems not to capture subsequent shifts in metabolic activities observed experimentally under low-nutrient regimes. Some discrepancies can be explained by the multiplicity of possible fermentative states for *F. prausnitzii*. In general, these results provide valuable guidelines for design of future experiments aimed at better determining the mechanisms leading to enhanced butyrate in this ecosystem.

Importance

Studies associating butyrate levels with human colonic health have inspired research on therapeutic microbiota consortia that would optimize butyrate production if implanted in the human colon. *Faecalibacterium prausnitzii* is commonly observed in human fecal samples and produces butyrate as a product of fermentation. Previous studies indicate that *Bacteroides thetaiotaomicron*, also commonly found in human fecal samples, may enhance butyrate production in *F. prausnitzi* when the two species are co-localized. This possibility is investigated here under different environmental conditions using experimental methods paired with computer simulations of the whole metabolism of bacterial cells. Initial findings indicate that interactions between these two species result in enhanced butyrate production. However, results also paint a nuanced picture, suggesting the existence of a multiplicity of equivalently efficient metabolic strategies and complex interactions between acetate and butyrate production in these species that appear highly dependent on specific environmental conditions.

Introduction

It is increasingly recognized that metabolites produced by the resident microbiota of the colon have a major influence on host physiology (1). Dietary substrates dramatically influence the amount and type of these metabolites produced (2). For instance, fermentation of carbohydrates produces a number of bioactive compounds, most notably short chain fatty acids (SCFA) such as butyrate, that have been demonstrated to shape the gut microenvironment, serve as an energy source for the colonic epithelium, and influence disease through anti-inflammatory, lipogenic, and anti-apoptotic effects (3–6).

The production of metabolites in a microbial community has been suggested to be heavily modulated by interactions among its members. These interactions manifest in a variety of modes, ranging from competitive or predatory to commensal and mutualistic exchanges (7). Additionally, many microbes in nature exist in spatially defined structures (8), such as the mucosal layer of the gut. Spatial assortment of cells creates locally heterogeneous subpopulations with varying access to resources that can also modulate inter- and intra-community behavior (9). A major goal of ongoing efforts in human microbiome research (10) is to gain enough predictive and quantitative understanding of inter-microbial interactions (11) and of the metabolic interplay between microbiota and host (12) to be able to understand the effects of the microbiome on human health. These capabilities could greatly facilitate successful design of therapeutic strategies for microbiome-related diseases.

Efforts towards safely, effectively and reliably engineering microbial communities (9) to improve human health are, however, limited by insufficient understanding of the nature of the mechanisms underlying microbial interactions and the way these interactions affect microbiome dynamics. Anaerobic *in vitro*, *in vivo* and *ex vivo* experiments capable of probing systems similar to the human colonic environment are difficult and expensive. Previous work uncovering fundamental properties of SCFA-producing bacteria and their symbiotic partners has used *Faecalibacterium prausnitzii* as a model system (13–21). This is motivated by the high prevalence of *F. prausnitzii* as a commensal bacterium in the human large intestine (22) and the role it plays as one of the major butyrate producers (23). Among the bacteria used for coculture studies, a common gut commensal, *Bacteroides thetaiotaomicron,* has been chosen in both experimental (24) and computational (25) analyses of SCFA production. In particular, experimental efforts to grow *F. prausnitzii* in coculture with *B. thetaiotaomicron* have suggested

89 enhancement of butyrate production in coculture relative to *F. prausnitzii* monoculture (24).
90 However, the data in this study was obtained only for a single time point and no information on
91 the dynamics of the biomass or butyrate production was provided. In general, to our knowledge,
92 no comparison has been previously made between experimentally measured time-courses of the
93 biomass of these species and their respective metabolic dynamics, when grown individually and
94 in co-culture.

95 In parallel, computational work based on metabolic network analyses has led to the
96 construction of genome scale models for each of these bacterial species, and to a computational
97 assessment of their metabolic capabilities (26–28). The modeling approach used in these studies,
98 often referred to as constraint-based modeling (or stoichiometric modeling) is based on
99 simplifying assumptions about the intracellular dynamics of metabolism. It enables quantitative
100 predictions of the intracellular and exchange fluxes, in addition to the growth rate of different
101 species. In particular, flux balance analysis (FBA) (29), can be used to calculate the flow of
102 metabolites through a metabolic network, making it possible to predict the growth rate of an
103 organism or the rate of production of important metabolites (30) (see also (31) for a
104 comprehensive review of different approaches). While the reconstructed networks and the
105 modeling tools used for making these predictions vary widely in accuracy and predictive power,
106 the formal representation of metabolism into these mathematical structures and codification of
107 multi-level processes into algorithms have sparked a revolution in systems biology of
108 metabolism, enabling precise hypothesis testing, and the formulation of genome-scale based
109 community modeling. In the context of human gut microbiome studies and inter-species
110 interactions, modeling work has been shown in particular to provide insight into the stability of
111 biofilm forming communities (25).

In order to make comparisons between computational predictions and experimental time-course data, it is important to be able to connect detailed knowledge of the intracellular metabolism of individual organisms to the dynamic metabolic changes occurring in the surrounding environment. An extension of FBA capable of these types of calculations is dynamic FBA (or dFBA)(32). Harcombe *et al.* (33) developed a computational framework specifically designed to help predict the spatio-temporal behavior of synthetic microbial consortia. This system, known as Computation of Microbial Ecosystems in Time and Space (COMETS) (33), generates predictions of biomass growth curves as well as detailed time dynamics of the concentrations of all nutrients and metabolites in the environment. COMETS has been shown to accurately predict the behavior of small artificial ecosystems.

Despite the availability of these experimental data and computational tools, many fundamental features of the interactions between *F. prausnitzii* and *B. thetaiotaomicron*, as well as our capacity to predict clinically relevant variables, remain unexplored. While previous studies have computationally and experimentally analyzed the metabolic capabilities of each of these bacteria individually (26, 27) and the dependence of these and other bacteria upon different oxygen levels (25), no direct comparison of experimental and computational time course data for this consortium under varying conditions has been presented before. In particular, no attempt has been made to recapitulate or predict these time-courses with dynamic computational models.

Here, we provide novel insight into the *F. prausnitzii* - *B. thetaiotaomicron* model system by combining new experimental measurements of bacterial biomass and environmental metabolites with COMETS-based computer simulations. We performed a series of anaerobic *in vitro* experiments involving monocultures and cocultures of *F. prausnitzii* and *B. thetaiotaomicron* grown in three different media, and found increased butyrate production in co-

136 culture relative to monoculture under high glucose and acetate concentrations. Upon fitting of six
137 parameters for metabolic uptake kinetics in monocolture, COMETS simulations were able to
138 recapitulate biomass time courses in monoculture and predict combined biomass time courses for
139 coculture. Model predictions for butyrate, however, portray a more complex picture. Accurate
140 predictions of initial butyrate production rate do not hold at longer times due to the existence of
141 multiple alternative optima in the flux states and the history-dependence of the dynamical
142 predictions. Strong sensitivity of the butyrate production curves to specific concentrations of
143 nutrients, including phosphate, provide insight into the complexity of these metabolic exchanges,
144 and valuable guidance for future experimental and modeling work.
145
146 **Results**
147 ***In vitro* and *in silico* coculture biomass dynamics under different nutrient limitations**
148 We initially characterized anaerobic growth of *B. thetaiotaomicron* and *F. prausnitzii*
149 individually and in coculture, under different levels of carbon availability (low, medium, high,
150 see Methods). In addition to glucose, acetate was added proportionally, mimicking the
151 fermentative activity of the rest of the microbiota (13). The presence of acetate in the medium
152 also allowed us to assess how, even in the absence of *B. thetaiotaomicron, F. prausnitzii*
153 responds to varying acetate availability.
154 Monoculture growth for *B. thetaiotaomicron* appears sensitive to the amount of carbon
155 provided (Fig. 1). Growth rate and yield increase in medium acetate/glucose medium compared
156 to low acetate/glucose concentrations. No clear increase in biomass occurred when carbon
157 abundance was increased from medium to high levels. The amount of *F. prausnitzii* biomass in
158 monoculture appears insensitive to increase in initial acetate/glucose levels. The combined

biomass growth curves of the coculture (measured as a collective OD) closely tracks OD curves of *B. thetaiotaomicron*, suggesting a prominent role of this bacterium in the consortium. This observation is consistent with previous experiments (3) in which the combined coculture biomass OD of *B. adolescentis* and *F. prausnitzii* mirrors the OD of the *B. adolescentis* monoculture, suggesting that some features of that consortium may be similar to the one studied here, even across different spatial scales and environmental settings.

In parallel to the experimental measurements, we implemented *in silico* simulations of the same monocultures and cocultures, using previously published genome-scale metabolic models for the two bacteria (26, 27). In particular, we used COMETS (33) to test whether (i) parameters from the literature, combined with minimal fitting of unknown parameters, would recapitulate the observed monoculture behavior and (ii) models tuned for monoculture experiments would be adequate to predict the outcome of the coculture experiment.

Superimposed on the experimental data, Fig. 1 shows the biomass dynamics as simulated in COMETS. The monoculture simulations were supplemented with empirical knowledge of uptake K_M and fitting of V_{max} values. After selecting initial kinetic parameter values based on previously determined corresponding parameters for the phosphotransferase (PTS) transporter (21, 34), a sensitivity analysis allowed us to identify V_{max} values that provide best fit of growth curves to monoculture (Fig. 2). This calibration step, similar to that previously performed in (35), produces simulated OD curves that broadly agree with the experimentally measured points (see root-mean-squared error (RMSE) in Table 1). Using these parameters for COMETS simulations of cocultures at the experimentally estimated initial biomass abundances, coculture predictions track coculture experimental data closely, as shown by predictive RMSE values (Table 1).

182

183 **Coculture conditions impact the average rate of butyrate production in experiments**

184 Throughout all of our experiments, in addition to monitoring the overall OD, we
185 measured the extracellular aboundance of butyrate and acetate. In Fig. 3, the average amount of
186 butyrate produced by *F. prausnitzii* in coculture appears higher than monoculture in the medium
187 and high initial acetate/glucose concentrations, but not in the low concentration conditions. In
188 low acetate/glucose conditions the butyrate production rate in coculture appears suppressed
189 relative to the one in monoculture. Box's approach in (36), applying ANOVA to summary
190 statistics describing growth curves, was used to quantify the statistical significance of the
191 difference in butyrate production curves across different treatments, i.e.: (i) monoculture vs.
192 coculture conditions (mono/co) and (ii) the three different initial acetate/glucose initial
193 concentrations (initial glu/ac). Tables 2 and 3 show that the average rate of butyrate production
194 in *F. prausnitzii* is significantly altered in mono vs. coculture conditions but not across the
195 different initial abundances of acetate and glucose. The initial acetate/glucose concentrations, but
196 not mono vs. coculture conditions, significantly change the average rate of acetate production
197 from *B. thetaiotaomicron*.

198 Interpretation of the above assessments of butyrate and acetate production is limited by
199 the lack of experimental knowledge of the precise amount of biomass of each species in the
200 coculture experiments**.** In particular, in absence of further laborious organism-specific data, it is
201 impossible to determine whether significant changes in the level of the butyrate curves are due to
202 *F. prausnitzii* producing more butyrate at the cellular level in the coculture, or whether the
203 increase is due to an increase in *F. prausnitzii* total biomass, enabled by coculture conditions, or
204 both. Under these circumstances, COMETS-predicted biomass estimates for each species from

coculture simulations (Fig. 6B) enabled hybrid computational-experimental estimates of biomass-normalized butyrate (Fig. 6A) and acetate (Fig. S2) production curves.

Trends of significance in Tables 5 and 6 for the normalized curves are similar to those for the unnormalized curves, with several exceptions. The average rate of both SCFAs are significantly affected by mono vs. coculture conditions in the normalized curves. These results imply that *B. thetaiotaomicron* stimulates butyrate production in *F. prausnitzii* on a per cell basis rather than by stimulating *F. prausnitzii* biomass production. *B. thetaiotaomicron* biomass-normalized acetate production curves are not significantly changed in average rate by initial glucose/acetate levels, in contrast to the non-normalized curves. As a note of caution, it is important to stress that the normalization relative to untested predicted abundances of individual species in co-culture should be considered putative. At the same time, it could be viewed as a valuable strategy for integrating experimental and computational data towards the formulation of new hypotheses.

The multiplicity of fermentation states with optimal efficiency influences SCFA time-course predictability

Figure 3 shows that COMETS accurately recapitulates the early stages of accumulation of extracellular butyrate. After 5 hours of growth, however, the picture becomes more complex. Simulation results at these times suggest that the regulation of butyrate and lactate pathways may play a major role in the final outcome of the secreted butyrate. To understand these results, the butyrate fermentation process in *F. prausnitzii* was revisited with additional computational analyses, specifically focused on alternative fermentation pathways. Three competing fermentation pathways exist in the curated metabolic network of *F. prausnitzii*. Pyruvate is fermented to one of the three products (27): (i) lactate, by D-lactate dehydrogenase

(reaction ID: LDH_D), (ii) formate, by pyruvate-formate lyase (reaction ID: PFL) or (iii) butyrate, by butyryl-CoA:acetate CoA-transferase (reaction ID: BTCOAACCOAT). Butyryl-CoA in turn is produced from acetyl-CoA (reaction ID: BTCOADH) and acetyl-CoA is converted from pyruvate by pyruvate:ferredoxin oxidoreductase (reaction ID: POR4i). The balance of metabolic flow through these three closely coupled fermentation pathways can significantly impact the production of butyrate in *F. prausnitzii,* depending on environmental conditions.

As shown in Figs. 3 and S4, and described in the methods section, COMETS, in its standard formulation, switches among these competing pathways. In particular, Figure S3 shows that *F. prausnitzii* switches from predominantly butyrate production activity at time zero to lactate secretion after 5 hours. This switch coincides with the transition from a single solution point of the FBA optimization at the early stages of the growth, to conditions where the FBA optimization algorithm has the freedom of choosing between a multitude of flux solution points, all corresponding to the same biomass growth rate. This multiplicity of equivalently efficient steady states (multiple alternative optima, also described in (37)) is best highlighted by systematically imposing, at each time point, additional features in the dFBA solution process. In particular, in analogy with flux variability analysis (38), we re-run the COMETS simulations by adding a secondary objective function at each time point. After maximizing for growth, the algorithm fixes the growth rate to the identified maximum, and subsequently searches for the solution that maximizes or minimizes the secretion flux of one of the organic acids, such as butyrate. Correspondingly, the butyrate secretion flux can be represented in the form of two curves of butyrate concentration extremes (Fig. 3). Notably, in most of the cases, the experimentally measured butyrate concentrations occupy a place between these two extremes. Nutrient limitations seem to be a strong determinant of this multiplicity of alternative optima.

252 The system is particularly sensitive to phosphate concentration, as shown in Figs. 4 and S4, and
253 is probably due to the strong coupling to phosphate in all butyrate producing pathways. These
254 simulation results therefore suggest that regulation of the fermentation pathways in *F. prausnitzii*
255 influence butyrate production under different environmental conditions.

256 The simulated acetate production shown in Fig. 5 tracks experimental time courses for
257 both *B. thetaiotaomicron* and *F. prausnitzii* monoculture, particularly in the medium and high
258 inital acetate/glucose conditions. Simulated time courses fall within error bars for average
259 experimental observations for all time points on the curves. The early stages of the coculture
260 simulations also closely track experiments. After 5 simulated hours, however, opposite trends in
261 acetate concentrations appear to mirror the discrepancies with experiment in the butyrate
262 simulations. While the experiments show depletion, the simulations result in buildup of acetate
263 in the late stages of the simulations. This inconsistency is also potentially explainable by a
264 metabolic switch in *F. prausnitzii*, resulting in less acetate consumption to produce butyrate.
265

266 **Discussion**

267 We analyzed experimentally and computationally the possible effects of a symbiotic
268 partner (*B. thetaiotaomicron*) and of environmental conditions (amount of glucose and acetate)
269 on the biomass of the gut bacterium *F.prausnitzii*, as well as its capacity to produce butyrate. In
270 monoculture, *F. prausnitzii* seems to continue producing butyrate even after the cells reach
271 stationary phase (at around 10 hours), suggesting that maintenance processes keep fueling the
272 butyrate production pathways. Another feature of the monoculture is the relatively low
273 sensitivity of biomass and butyrate production to glucose and acetate concentrations. In contrast,
274 biomass and butyrate seem to more strongly depend on the environment in the presence of *B.*

thetaiotaomicron in the coculture experiments (Figure 3), although this difference is not statistically significant, based on ANOVA.

The possibility of metabolic cross-feeding between *F. prausnitzii* and *B. thetaiotaomicron* has been suggested in previous studies (24). In some of these studies, acetate production by *B. thetaiotaomicron* is proposed to mediate the interaction between the two bacteria, facilitating an increased butyrate production by *F. prausnitzii*. While it is likely that indeed acetate plays a key role in the interaction between the two bacteria, the results of our study suggest a more complex mode of interaction: First, the statistically significant increase in butyrate production we observe in coculture does not seem to increase monotonically with the amount of glucose and acetate, suggesting that either the two carbon sources are saturated (24), or that acetate exchange is not the only factor dominating butyrate production. Second, as demonstrated by our COMETS dFBA simulations, the stoichiometry of *F. prausnitzii* suggests that multiple alternative growth optima are possible (depending on whether or not other nutrients – most notably phosphate – are limiting in the medium). These different optima can differ substantially in their combination of fermentation products, thus making the stoichiometry-based prediction of a specific rate of butyrate production impossible. Instead, only a range of production rates can be predicted at any given time. This hypothesized degree of freedom in fermentative pathways could in principle be used by *F. prausnitzii* to modulate its metabolic activity and its butyrate production rate in response to external signals. Future studies using dFBA for studying *F. prausnitzii* could use additional constraints (e.g. total flux capacity (38) or

regulatory information (38)) to refine the predictions, and to systematically test the effect of different nutrient limitations and growth media on butyrate production.

In this work, COMETS predictions were also used to estimate relative biomass amount of the two species in coculture, in the absence of experimental observations. Although the accuracy of the COMETS relative biomass estimates were not confirmed using experimental data, its ability to predict the total biomass in coculture using parameters learned from monoculture conditions lends credence to these estimates. Follow-up experiments to fully vet model accuracy in determining relative biomass in consortia would be invaluable towards building confidence in hybrid computational-experimental approaches like the one demonstrated here.

Methods and Materials

COMETS Simulation Configuration The metabolic network models we use in this work for *Bacteroides thetaiotaomicron* strain VPI-5482 and *Faecalibacterium prausnitzii* strain A2-165 were published and made publicly available by Heinken *et al.* in (26) and (27). The COMETS simulation framework is implemented in Java and described in (33). R and Matlab scripts transform COMETS outputs to time-course plots. The 3D volume in these simulations contains 5 mL of isotropic medium and biomass. COMETS' ability to model spatial differences in microbial systems is not explored in these preliminary simulations. Similarly, the dFBA settings, other than the ones mentioned below, were set at their default values as implemented in COMETS. The FBA parsimonious optimization was performed using the GUROBI optimizer, with a primary maximization of the biomass growth rate and a secondary minimization of the absolute values sum of the metabolic fluxes. The butyrate secretion analysis also included

additional maximization and/or minimization of butyrate, lactate and formate uptake. Simulation run time was 24 hours, with each time step set to 0.01 hour. The death rate was set to zero.

The uptake of nutrients was modeled as a saturation Michaelis-Menten curve with two adjustable parameters, maximum uptake flux, V_{max}, and the Michaelis constant K_M. Our choice of parameters for the uptake curve was guided by values provided in the original publications of the models and as reported in the literature (39, 40). The glucose uptake in *F. prausnitzii,* for example, is governed by PTS transporter (27) with reported K_M values up to 8.7 mM (34). These starting values for the uptake parameters where additionally fine-tuned by fitting the single-species simulations results for the OD to the corresponding experimental curves. **Error! Reference source not found.** shows the fitting procedure for *B. thetaiotaomicron* and *F. prausnitzii* respectively. In the case of *B. thetaiotaomicron* a single value for the maximum uptake parameter was sufficient to fit the growth curves. The accepted value minimized the composite reduced chi-squared for all three growth conditions. In the case of *F. prausnitzii*, we used two values for the maximum uptake. Starting with the value for K_M we fitted the glucose and acetate uptake, and then performed a fine tuning for the rest of the metabolites/nutrients. Parameter values are shown in Table 6.

Metabolic activity in the *F. prausnitzii* model showed a nutrient concentration dependent shift, most sensitive to phosphate depletion, from butyrate producing pathway, to a lactate producing one, shown in Fig. S3. This shift is characterized by a single solution point of the FBA optimization sequence, both for minimized and maximized butyrate secretion, at high values of phosphate concentration, shown in Fig. S4, corresponding to the initial time in the dFBA simulation. As the substrate is depleted of the nutrients, the system obtains multiple optimal solution points, with the difference in the butyrate production depending on the

341 secondary optimization of butyrate secretion (Fig. S4) providing a range of possible butyrate
342 secretion rates at the later stages of the dFBA simulations. The complete set of input as well as
343 simulations output files can be found in the supplement. COMETS is available to download at
344 comets.bu.edu.
345
346 ***ANOVA Methodology*** Box's method (36) for describing and quantifying differences in growth
347 curves was implemented as follows. The average rate/level statistic is computed as the average
348 of the measurements from the first time point concentration measurement subtracted from the
349 average of the measurements from the last divided by the total time. The rate of butyrate
350 production for each time bin was computed similarly and the average rate was subtracted from
351 these for the set of rate deviations that define the shape statistic.
352 We use the Bonferonni corrected significance level of 0.0042 in this study with twelve
353 comparisons (six per metabolite) to conservatively approximate the 0.05 significance level in
354 single comparisons. The small number of replicates in our study (3 replicates), results in
355 relatively low power for ANOVA tests. Insignificant results in our ANOVA analysis may
356 therefore derive from low power, randomness or some combination of the two (41) for both the
357 *shape* and *level* ANOVA results. Additionally, violations of homogeneous measurement
358 covariance matrices and/or normally distributed prediction errors with zero mean could also
359 result in pessimistically biased significance estimates. In particular, violation of homogeneous
360 covariance matrices may negatively bias *shape* ANOVA results (42). ANOVA results for *level*
361 have been shown to be robust to violations of this assumption (43).
362 We did not test our data for violations of these two conditions because tests for normality
363 and equal variance are themselves inconclusive with small sample sizes. Given that violations of

364 homogeneous measurement covariance matrices can negatively bias significance results in *shape*
365 ANOVA, the insignificant results in this study should be probed further with larger sample sizes.
366 Because *level* ANOVA results have been shown to be robust to violations of homogeneous
367 measurement covariance matrices (43), we are confident in the finding of significant differences
368 between monoculture and coculture metabolite production curves in *level*/average rate. As is
369 always the case, however, follow-up studies with larger sample sizes would be advised to both
370 test reproducibility and lend more power to ANOVA results.
371
372 ***In Vitro Experimental Configuration/OD600 Analysis*** Bacteria were cultured in Yeast
373 Casitone (YC) medium, with three different concentrations of supplemented acetic acid/glucose.
374 "Low" condition: 5.551mM acetic acid, .1% glucose. "Medium" condition: 27.754mM acetic
375 acid, .5% glucose. "High" condition: 55.507mM acetic acid, 1% glucose. All media were
376 adjusted to pH 6.8 before autoclaving.
377 Bacterial cultures were started in anaerobic conditions from glycerol stocks stored at -
378 80°C in 3mL of "Medium" YC medium. After overnight culture, OD600 was measured, and the
379 cultures were diluted to the nominal OD starting points in 5mL of the three different YC
380 formulations.
381 The following cultures were started with the initial OD600 values as noted:
382 OD600 ~.02 *B. thetaiotamicron* monoculture
383 OD600 ~.08 *F. prausnitzii* monoculture
384 OD600 ~.02 *B. thetaiotamicron* AND OD600 ~.08 *F. prausnitzii* coculture
385 A baseline 200µL aliquot was taken from each culture, measured by OD600, and stored
386 at -80 for later MS analysis. Subsequent 200µL aliquots were collected and measured by OD600

387 at 2, 4, 6, 8, 10 and 24 hours and stored for later analysis. The above procedure was repeated in
388 triplicate, yielding three observations per time point.
389
390 ***MSMS Analysis*** A flow injection analysis electrospray ionization mass spectrometry (FIA ESI
391 MSMS) method was used for quantitative detection of short chain fatty acids (SCFA). Acetic,
392 propionic, butyric and succinic acid were derivatized with 3-nitrophenylhydrazine in the
393 presence of N-(3-dimethylaminopropyl)-N'-ethylcarbodiimide and pyridine and detected by a
394 mass spectrometer as a 3-nitrophenylhydrozones in MRM (multiple reaction monitoring) MSMS
395 mode, as described by J. Han *et al.* (44). To increase precision and robustness of the method, 3-
396 methylbutyric-2-2-d2 acid , acetic acid-2-13C and propionic acid -1-13C were used as an
397 internal standards. Quantitation was done by external standards calibration, where instrument
398 response for the analyte was measured as a ratio between analyte's and internal standard's peak
399 areas. The FIA technique did not utilize LC column but rather a direct injection of the sample
400 into an ESI probe of the mass spectrometer and this decreased time of analysis per sample to two
401 minutes. The FIA ESI MSMS for the detection of SCFA is sensitive with the limit of detection
402 for acetic, propionic, butyric and succinic acids at 4, 3, 0.6 and 1.4µM respectively. The
403 accuracy of the method was between 98-102%.
404
405 ***Reagents*** LC MS grade acetonitrile and water were purchased from VWR (Radnor, PA, USA).
406 N-(3-dimethylaminopropyl)-N'-ethylcarbodiimide HCl, 3-nitrophenylhydrazine HCl, pyridine,
407 acetic acid, propionic acid, butyric acid, succinic acid, acetic acid 13C, and propionic acid 13C
408 were purchased from Sigma-Aldrich (St Luis, MO, USA). 3-methylbutyric-2-2-d2 acid was
409 purchased from CDN Isotopes (Quebec, CN).

410

411 ***FIA MS/MS system*** An Agilent infinity capillary LC pump with micro-autosampler and
412 thermostat (Agilent Technologies, Santa Clara, CA, USA) coupled to AB Sciex 4000 Q-TRAP
413 triple- quadrupole mass spectrometer (AB Sciex, Concord, Ontario, CN) was used for the
414 analysis. The flow solvent - five percent water and ninety five percent acetonitrile was delivered
415 to a mass spectrometer ESI probe at the rate of 350µL/min. Samples for flow injection analysis
416 were derivatized on the Agilent polypropylene 96 well plate and injected into mass spectrometer
417 with injection volume of 40µL. Following conditions for the AB Sciex Q-TRAP 4000 were used
418 for analysis: source temperature 400°C, source gas 40L/min, curtain gas 10L/min, ESI capillary
419 voltage was set at –4500 volts. Data were acquired in negative polarity multiple reactions
420 monitoring (MRM) mode for the MRM transitions specified in the Table S1.

421

422 **Data Availability**

423 Data files and scripts used to generate the figures presented in this paper can be found in a zipped
424 directory (Yu_etal_Data_and_Scripts.zip) downloadable at https://github.com/segrelab/Fprau-
425 Btheta-2018. This directory contains the experimental data and script for statistical analysis and
426 for generating the figures (DATA_AND_FIGURE_SCRIPTS subdirectory), and COMETS input
427 and output files (SIMULATIONS_INPUTS_AND_OUTPUTS subditrectory). The *in silico*
428 experiments were generated using COMETS v.2.5.8, which is freely available at
429 http://comets.bu.edu.

430

431 **Acknowledgements**

DS and ID acknowledge funding from the Defense Advanced Research Projects Agency (Purchase Request No. HR0011515303, Contract No. HR0011-15-C-0091), the NIH (5R01DE024468, R01GM121950 and Sub_P30DK036836_P&F), and the Boston University Interdisciplinary Biomedical Research Office. This material is based upon work supported by the Assistant Secretary of Defense for Research and Engineering under Air Force Contract No. FA8702-15-D-0001. Any opinions, findings, conclusions or recommendations expressed in this material are those of the author(s) and do not necessarily reflect the views of the Assistant Secretary of Defense for Research and Engineering.

References

1. Lozupone CA, Stombaugh JI, Gordon JI, Jansson JK, Knight R. 2012. Diversity, stability and resilience of the human gut microbiota. Nature 489:220–230.

2. Yatsunenko T, Rey FE, Manary MJ, Trehan I, Dominguez-Bello MG, Contreras M, Magris M, Hidalgo G, Baldassano RN, Anokhin AP, Heath AC, Warner B, Reeder J, Kuczynski J, Caporaso JG, Lozupone CA, Lauber C, Clemente JC, Knights D, Knight R, Gordon JI. 2012. Human gut microbiome viewed across age and geography. Nature 486:222–227.

3. Rios-Covian D, Gueimonde M, Duncan SH, Flint HJ, De Los Reyes-Gavilan CG. 2015. Enhanced butyrate formation by cross-feeding between Faecalibacterium prausnitzii and Bifidobacterium adolescentis. FEMS Microbiol Lett 362:1–7.

4. Canani RB, Costanzo M Di, Leone L, Pedata M, Meli R, Calignano A. 2011. Potential beneficial effects of butyrate in intestinal and extraintestinal diseases. World J Gastroenterol 17:1519–1528.

5. Flint HJ, Duncan SH, Scott KP, Louis P. 2015. Links between diet, gut microbiota

composition and gut metabolism. Proc Nutr Soc 74:13–22.

6. Lopez-Siles M, Khan TM, Duncan SH, Harmsen HJM, Garcia-Gil LJ, Flint HJ. 2012. Cultured representatives of two major phylogroups of human colonic Faecalibacterium prausnitzii can utilize pectin, uronic acids, and host-derived substrates for growth. Appl Environ Microbiol 78:420–428.

7. Mitri S, Richard Foster K. 2013. The Genotypic View of Social Interactions in Microbial Communities. Annu Rev Genet 47:247–273.

8. Kolter R, Greenberg EP. 2006. Microbial sciences: The superficial life of microbes. Nature 441:300–302.

9. Johns NI, Blazejewski T, Gomes ALC, Wang HH. 2016. Principles for designing synthetic microbial communities. Curr Opin Microbiol 31:146–153.

10. Turnbaugh PJ, Ley RE, Hamady M, Fraser-Liggett CM, Knight R, Gordon JI. 2007. The Human Microbiome Project. Nature 449:804–810.

11. Venturelli OS, Carr AC, Fisher G, Hsu RH, Lau R, Bowen BP, Hromada S, Northen T, Arkin AP. 2018. Deciphering microbial interactions in synthetic human gut microbiome communities. Mol Syst Biol 14:e8157.

12. Nicholson JK, Holmes E, Kinross J, Burcelin R, Gibson G, Jia W, Pettersson S. 2012. Metabolic Interactions 108:1262–1268.

13. Belzer C, Chia LW, Aalvink S, Chamlagain B, Piironen V, Knol J, de Vos WM. 2017. Microbial metabolic networks at the mucus layer lead to diet-independent butyrate and vitamin B12production by intestinal symbionts. MBio 8:1–14.

14. Das P, Ji B, Kovatcheva-Datchary P, Bäckhed F, Nielsen J. 2018. In vitro co-cultures of human gut bacterial species as predicted from co-occurrence network analysis. PLoS One

13:1–14.

15. Duncan SH, Barcenilla A, Stewart CS, Pryde SE, Flint HJ. 2002. Acetate utilization and butyryl coenzyme A (CoA): Acetate-CoA transferase in butyrate-producing bacteria from the human large intestine. Appl Environ Microbiol 68:5186–5190.

16. Louis P, Flint HJ. 2009. Diversity, metabolism and microbial ecology of butyrate-producing bacteria from the human large intestine. FEMS Microbiol Lett 294:1–8.

17. Miquel S, Martin R, Bridonneau C, Robert V, Sokol H, Bermúdez-Humarán LG, Thomas M, Langella P. 2014. Ecology and metabolism of the beneficial intestinal commensal bacterium Faecalibacterium prausnitzii. Gut Microbes 5.

18. Prévoteau A, Geirnaert A, Arends JBA, Lannebère S, Van De Wiele T, Rabaey K. 2015. Hydrodynamic chronoamperometry for probing kinetics of anaerobic microbial metabolism - Case study of Faecalibacterium prausnitzii. Sci Rep 5:1–13.

19. Sokol H, Pigneur B, Watterlot L, Lakhdari O, Bermudez-Humaran LG, Gratadoux J-J, Blugeon S, Bridonneau C, Furet J-P, Corthier G, Grangette C, Vasquez N, Pochart P, Trugnan G, Thomas G, Blottiere HM, Dore J, Marteau P, Seksik P, Langella P. 2008. Faecalibacterium prausnitzii is an anti-inflammatory commensal bacterium identified by gut microbiota analysis of Crohn disease patients. Proc Natl Acad Sci 105:16731–16736.

20. Tremaroli V, Bäckhed F. 2012. Functional interactions between the gut microbiota and host metabolism. Nature 489:242–249.

21. Stewart CS, Hold GL, Duncan SH, Flint HJ, Harmsen HJM, Hold GL, Harmsen HJM, Stewart CS, Flint HJ. 2002. Growth requirements and fermentation products of *Fusobacterium prausnitzii*, and a proposal to reclassify it as *Faecalibacterium prausnitzii* gen. nov., comb. nov. Int J Syst Evol Microbiol 52:2141–2146.

502 22. Maier, Eva. 2017. Effect of Faecalibacterium prausnitzii on intestinal barrier function and
503 immune homeostasis.
504 23. Vital M, Karch A, Pieper DH. 2017. Colonic Butyrate-Producing Communities in
505 Humans: an Overview Using Omics Data. mSystems 2:e00130-17.
506 24. Wrzosek L, Miquel S, Noordine ML, Bouet S, Chevalier-Curt MJ, Robert V, Philippe C,
507 Bridonneau C, Cherbuy C, Robbe-Masselot C, Langella P, Thomas M. 2013. Bacteroides
508 thetaiotaomicron and Faecalibacterium prausnitzii influence the production of mucus
509 glycans and the development of goblet cells in the colonic epithelium of a gnotobiotic
510 model rodent. BMC Biol 11.
511 25. Henson M, Phalak P. 2017. Byproduct Cross Feeding and Community Stability in an In
512 Silico Biofilm Model of the Gut Microbiome. Processes 5:13.
513 26. Heinken A, Sahoo S, Fleming RMT, Thiele I. 2013. Systems-level characterization of a
514 host-microbe metabolic symbiosis in the mammalian gut. Gut Microbes 4.
515 27. Heinken A, Khan MT, Paglia G, Rodionov DA, Harmsen HJM, Thiele I. 2014. Functional
516 metabolic map of Faecalibacterium prausnitzii, a beneficial human gut microbe. J
517 Bacteriol 196:3289–3302.
518 28. El-Semman IE, Karlsson FH, Shoaie S, Nookaew I, Soliman TH, Nielsen J. 2014.
519 Genome-scale metabolic reconstructions of Bifidobacterium adolescentis L2-32 and
520 Faecalibacterium prausnitzii A2-165 and their interaction. BMC Syst Biol 8:1–11.
521 29. Orth JD, Thiele I, Palsson BØ. 2010. What is flux balance analysis? Nat Biotechnol
522 28:245–8.
523 30. Feist AM, Zielinski DC, Orth JD, Schellenberger J, Markus J, Palsson BØ. 2011. Model-
524 driven evalution of the production potential for growth coupled products of Escherichia

525 coli. Metab Eng 12:173–186.

526 31. Zomorrodi AR, Segrè D. 2016. Synthetic ecology of microbes: mathematical models and
527 applications Graphical Abstract HHS Public Access. J Mol Biol J Mol Biol Febr Pt B
528 27:837–861.

529 32. Mahadevan R, Edwards JS, Doyle FJ. 2002. Dynamic Flux Balance Analysis of diauxic
530 growth in Escherichia coli. Biophys J 83:1331–1340.

531 33. Harcombe WR, Riehl WJ, Dukovski I, Granger BR, Betts A, Lang AH, Bonilla G, Kar A,
532 Leiby N, Mehta P, Marx CJ, Segrè D. 2014. Metabolic resource allocation in individual
533 microbes determines ecosystem interactions and spatial dynamics. Cell Rep 7:1104–1115.

534 34. Castro R, Neves AR, Fonseca LL, Pool WA, Kok J, Kuipers OP, Santos H. 2009.
535 Characterization of the individual glucose uptake systems of Lactococcus lactis: Mannose-
536 PTS, cellobiose-PTS and the novel GlcU permease. Mol Microbiol 71:795–806.

537 35. Louca S, Doebeli M. 2015. Calibration and analysis of genome-based models for
538 microbial ecology. Elife 4:1–17.

539 36. Box GEP. 1950. Problems in the Analysis of Growth and Wear Curves Author (s): G . E
540 . P . Box Published by : International Biometric Society Stable URL :
541 http://www.jstor.org/stable/3001781 REFERENCES Linked references are available on
542 JSTOR for this article : You may. Biometrics 6:362–389.

543 37. Segre D, Vitkup D, Church GM. 2002. Analysis of optimality in natural and perturbed
544 metabolic networks. Proc Natl Acad Sci 99:15112–15117.

545 38. Mahadevan R, Schilling CH. 2003. The effects of alternate optimal solutions in constraint-
546 based genome-scale metabolic models. Metab Eng 5:264–276.

547 39. Meadows AL, Karnik R, Lam H, Forestell S, Snedecor B. 2010. Application of dynamic

548 flux balance analysis to an industrial Escherichia coli fermentation. Metab Eng 12:150–
549 160.
550 40. Jahreis K, Pimentel-Schmitt EF, Brückner R, Titgemeyer F. 2008. Ins and outs of glucose
551 transport systems in eubacteria. FEMS Microbiol Rev 32:891–907.
552 41. Hewitt CE, Mitchell N, Torgerson DJ, Hewitt C, Torgerson D. 2008. significant
553 Unexpected non-significant results from randomised trials can be difficult to accept . 23–
554 25.
555 42. Snee RD. 1972. American Society for Quality On the Analysis of Response Curve Data
556 On the Analysis of Response Curve Data. Source: Technometrics 14:47–62.
557 43. Grenhouse, Samuel W. Geisser S. 1959. ON METHODS IN THE ANALYSIS OF
558 PROFILE variance . Furthermore , an analysis of variance approach permits the analysis
559 of a set of data which cannot be handled by multivariate procedures , namely , the case
560 where n , the number of random vectors , is less t. Phychometrika 24:95–112.
561 44. Han J, Lin K, Sequeira C, Borchers CH. 2015. An isotope-labeled chemical derivatization
562 method for the quantitation of short-chain fatty acids in human feces by liquid
563 chromatography-tandem mass spectrometry. Anal Chim Acta 854:86–94.
564
565
566 **Tables:**
567

	Low	Medium	High
Coculture	0.110	0.071	0.049
B. thetaiotaomicron	0.034	0.065	0.112
F. prausnitzii	0.064	0.094	0.043

568

569 **Table 1**. Table of RMSE between the values in Fig. 1 measured experimentally and predicted by
570 simulations, for monocultures and coculture in three carbon source conditions as described in the
571 text.

572
573

	Acetate					Butyrate				
Source	Sum Sq.	d.f.	Mean Sq.	F	Prob>F	Sum Sq.	d.f.	Mean Sq.	F	Prob>F
initial glc/ac	21.14	2	10.571	0.47	0.6277	1.3206	2	0.66032	0.69	0.5015
mono/co	115.13	1	115.131	5.1	0.0261	0.11956	1	0.11945	0.13	0.7237
initialglc/ac*mono/co	76.86	2	38.43	1.7	0.1877	0.275	2	0.13751	0.14	0.8655
Error	2304.56	102	22.594			96.9437	102	0.95043		
Total	2517.69	107				98.6588	107			

574
575 **Table 2**. Analysis of Variance of Shape of Metabolite Curves.

576
577

	Acetate					Butyrate				
Source	Sum Sq.	d.f.	Mean Sq.	F	Prob>F	Sum Sq.	d.f.	Mean Sq.	F	Prob>F
initial glc/ac	20.8263	1	20.8263	17.66	0.0012	0.17635	1	0.17635	4.29	0.0606
mono/co	1.6629	2	0.8315	0.7	0.5135	2.09982	2	1.04991	25.53	0
initialglc/ac*mono/co	13.2214	2	6.6107	5.61	0.0191	0.41137	2	0.20568	5	0.0263
Error	14.1527	12	1.1794			0.49346	12	0.04112		
Total	49.8634	17				3.181	17			

578
579 **Table 3**. Analysis of Variance of Average Rate of Metabolite Curves.

580

581

	Acetate					Butyrate				
Source	Sum Sq.	d.f.	Mean Sq.	F	Prob>F	Sum Sq.	d.f.	Mean Sq.	F	Prob>F
initial glc/ac	1.81E+07	2	9.06E+06	0.08	0.9272	2745098	2	1372549	0.46	0.6328
mono/co	4.80E+06	1	4.80E+06	0.04	0.8417	25019.6	1	25019.6	0.01	0.9272
initialglc/ac*mono/co	9.61E+06	2	4.81E+06	0.04	0.9606	953798	2	476899	0.16	0.8526
Error	1.22E+10	102	1.20E+08			3E+08	102	2985539		
Total	1.23E+10	107				3.1E+08	102			

582
583 **Table 4**. Analysis of Variance of Average Rate of Metabolite Curves.

584

	Acetate	Butyrate

Source	Sum Sq.	d.f.	Mean Sq.	F	Prob>F	Sum Sq.	d.f.	Mean Sq.	F	Prob>F
initial glc/ac	162363.1	1	162363.1	1.57	0.234	11506.9	1	11506.9	0.2	0.6612
mono/co	3919429.3	2	1959714.6	18.96	0.0002	1156514	2	578257	10.15	0.0026
initialglc/ac*mono/co	2590821	2	1295410.5	12.53	0.0012	517152	2	258576	5.54	0.0341
Error	12640529.9	12	103377.5			683892	12	56991		
Total	7913143.3	17				2369065	17			

Table 5. Analysis of Variance of Average Rate of Biomass-Normalized Metabolite Curves.

Species	*Vmax*[mmol/hg]	Glc./Ac.*Vmax*[mmol/hg]	*Km* [mM]	Glc./Ac. *Km* [mM]
B.thetaiotaomicoron	11	11	3	3
F. prausnitzii	23	10	10	5

Table 6. Parameters of the Michaelis-Menten uptake functions. Glucose and acetate uptake parameters were obtained independently from the rest of the nutrients for the model of *F. prausnitzii.*

Supplemental table legend:

Table S1. AB Sciex 4000-TRAP parameters used for detection of SCFA Q1 – m/z of the analyte ion detected on the 1rst quadrupole.Q3 – m/z of the anatyte's fragment ion detected on the third quadrupole. DP- declustering potential, CE – collision energy. Analytes in red are internal standards.

Figure legends:

Figure 1. Optical densities for single species and coculture of *F. prausnitzii* and *B. thetaiotaomicron*, grown in three different media conditions. The simulations (solid curves) were

602 obtained by dFBA with the same set of uptake parameters for all media conditions. The columns
603 correspond to the media conditions while the rows correspond to the cultured species.

604

605 **Figure 2**. The sensitivity of the OD curves to the values of the maximum nutrient uptake
606 parameter V_{max}. The values of the V_{max} parameter used in the simulations were obtained by
607 minimizing χ^2,the sum of the squared deviations of the simulation from the experimental values,
608 weighted by the measured variance. We used a single value of V_{max} for the uptake of all
609 nutrients by the *B. thetaiotaomicron* model, with the minimum of minimizing χ^2, shown in panel
610 A). In the case of *F. prausnitzii*, we determined two separate values of minimizing χ^2, one for
611 glucose and acetate uptake shown on panel B), and another one for the rest of the nutrients,
612 shown on panel C).

613

614 **Figure 3**. Experimental and simulated (solid, dot and dash curves) butyrate production
615 time courses for monocultures and coculture under the three initial glucose/acetate initial
616 concentrations. Apparent differences demonstrated in these plots in butyrate production for F.
617 prausnitzii monoculture vs. coculture and for the three initial concentrations can be tested
618 statistically using ANOVA on summary statistics describing the curves. The simulated curves
619 correspond to the maximized (solid curve) and minimized (dash dot curve) butyrate secretion.

620

621 **Figure 4**. Simulated butyrate production for three starting abundances of phosphate for
622 the low initial acetate/glucose concentration. Lowering of the phosphate concentration leads to
623 multiple FBA solutions and difference between secondary minimization and maximization of
624 butyrate secretion.

625

626 **Figure 5**. Experimental and simulated (solid curves) acetate production time courses for
627 monocultures and coculture under the three initial glucose/acetate initial concentrations.
628 Apparent differences demonstrated in these plots in butyrate production for *F. prausnitzii*
629 monoculture vs. coculture and for the three initial concentrations can be tested statistically using
630 ANOVA on summary statistics describing the curves.

631

632 **Figure 6**. A) Butyrate concentration time profile, normalized by the simulated *F.*
633 *prausnitzii* biomass, for coculture and monoculture. B) Simulated species composition.

634

635 **Supplemental figure legends:**

636 **Figure S1**. Simulated glucose concentration.

637 **Figure S2**. Biomass normalized acetate concentration.

638 **Figure S3**. Simulated fluxes of key reactions in the butyrate fermentation pathway in *F.*
639 *prausnitzii,* for high glucose concentration, at time zero and 5 hours.

640 **Figure S4**. Simulated butyrate secretion fluxes in *F. prausnitzii*, under secondary
641 maximization/minimization of butyrate or lactate production, as a function of phosphate
642 concentration, in low glucose conditions.

643

644

645

646

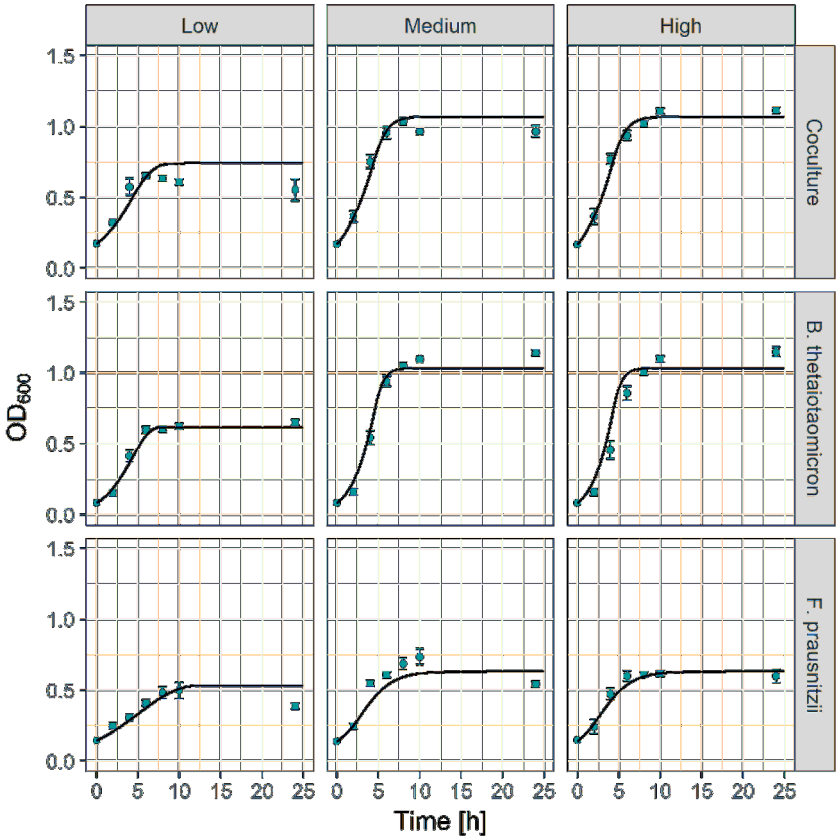

Figure 1. Optical densities for single species and coculture of *F. prausnitzii* and *B. thetaiotaomicron*, grown in three different media conditions. The simulations (solid curves) were obtained by dFBA with the same set of uptake parameters for all media conditions. The columns correspond to the media conditions while the rows correspond to the cultured species.

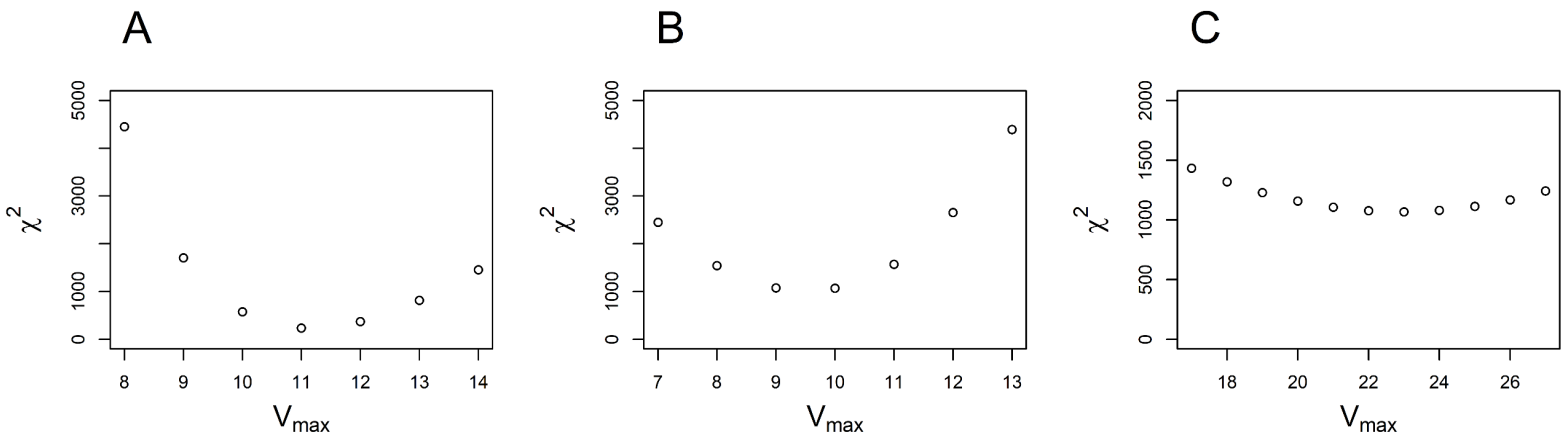

Figure 2. The sensitivity of the OD curves to the values of the maximum nutrient uptake parameter V_{max}. The values of the V_{max} parameter used in the simulations were obtained by minimizing c^2,the sum of the squared deviations of the simulation from the experimental values, weighted by the measured variance. We used a single value of V_{max} for the uptake of all nutrients by the *B. thetaiotaomicron* model, with the minimum of minimizing c^2, shown in panel A). In the case of *F. prausnitzii*, we determined two separate values of minimizing c^2, one for glucose and acetate uptake shown on panel B), and another one for the rest of the nutrients, shown on panel C).

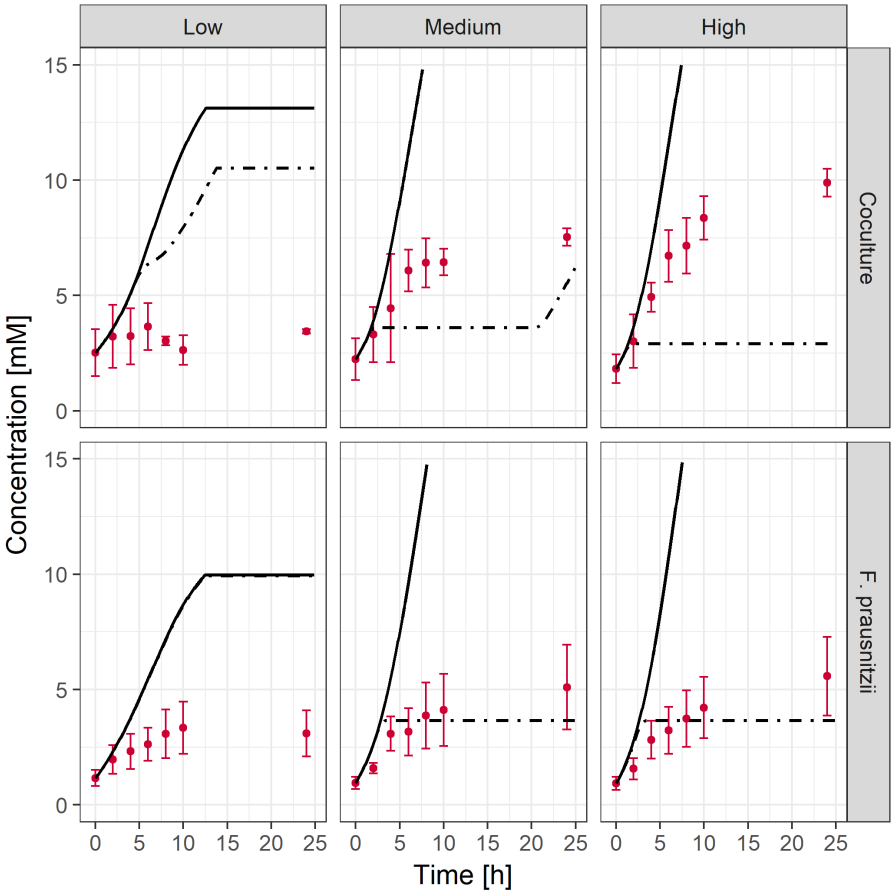

Figure 3. Experimental and simulated (solid, dot and dash curves) butyrate production time courses for monocultures and coculture under the three initial glucose/acetate initial concentrations. Apparent differences demonstrated in these plots in butyrate production for *F. prausnitzii* monoculture vs. coculture and for the three initial concentrations can be tested statistically using ANOVA on summary statistics describing the curves. The simulated curves correspond to the maximized (solid curve) and minimized (dash dot curve) butyrate secretion.

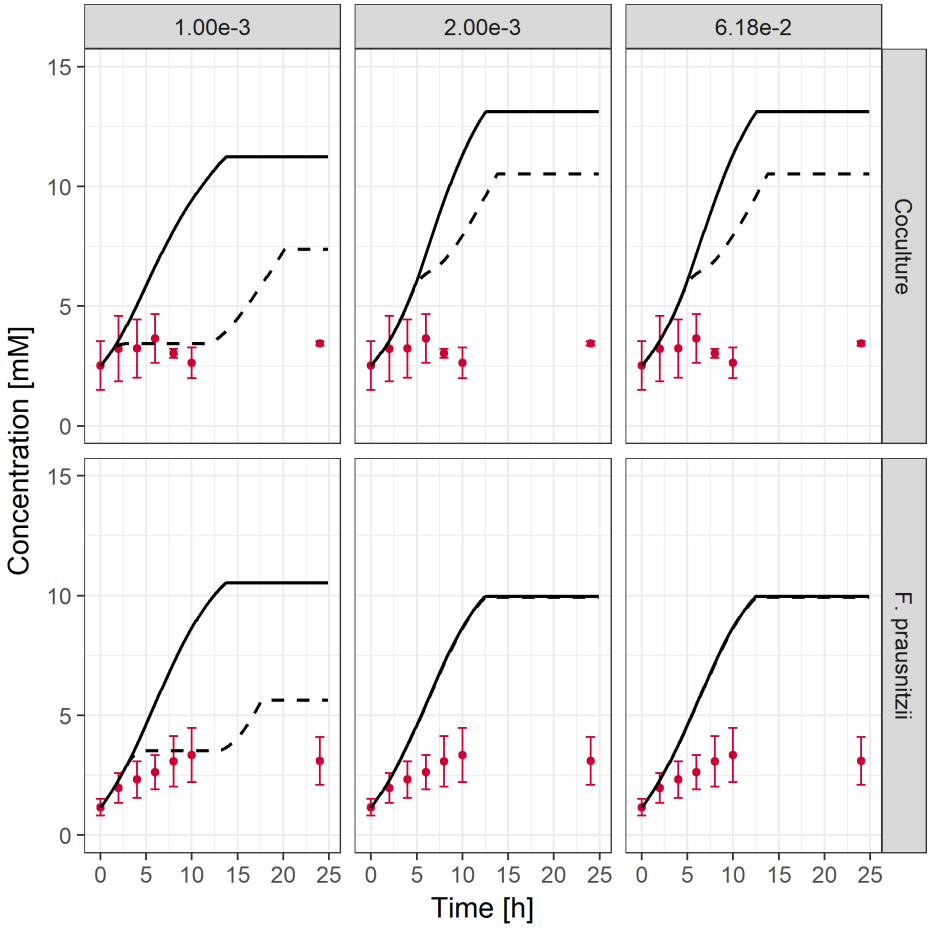

Figure 4. Simulated butyrate production for three starting abundances of phosphate for the low initial acetate/glucose concentration. Lowering of the phosphate concentration leads to multiple FBA solutions and difference between secondary minimization and maximization of butyrate secretion.

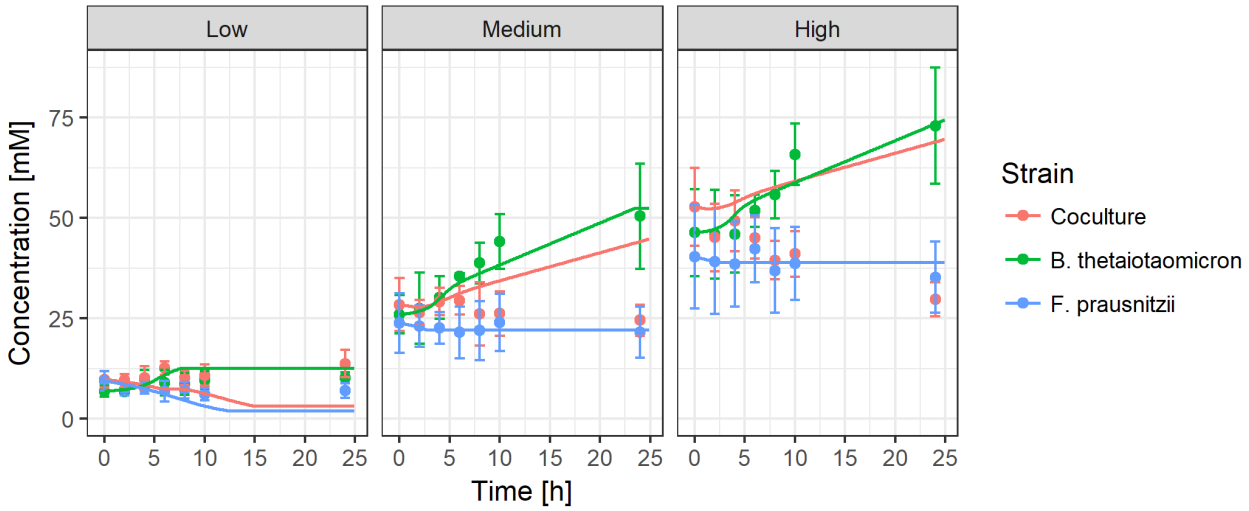

Figure 5. Experimental and simulated (solid curves) acetate production time courses for monocultures and coculture under the three initial glucose/acetate initial concentrations. Apparent differences demonstrated in these plots in butyrate production for *F. prausnitzii* monoculture vs. coculture and for the three initial concentrations can be tested statistically using ANOVA on summary statistics describing the curves.

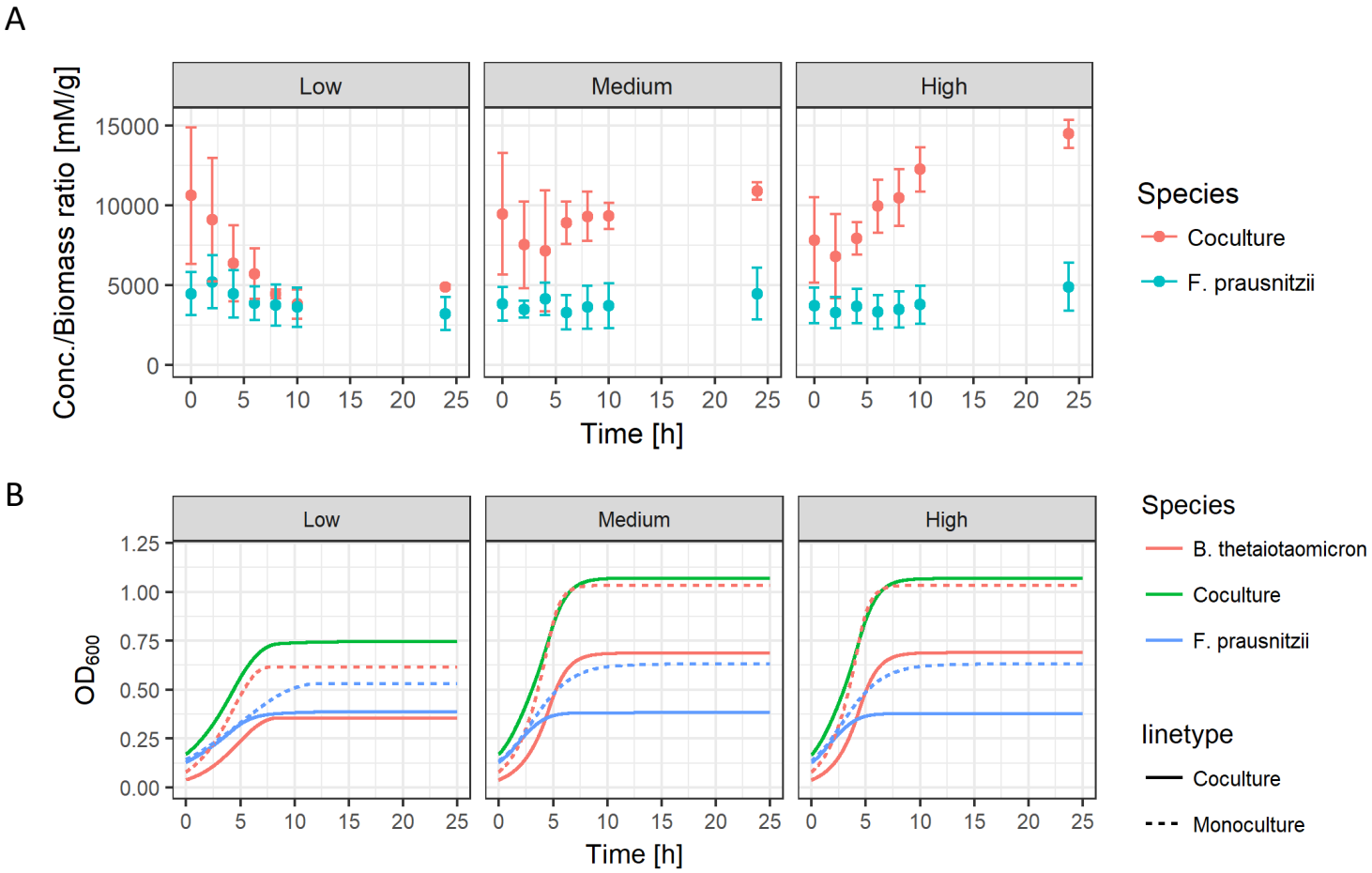

Figure 6. A) Butyrate concentration time profile, normalized by the simulated *F. prausnitzii* biomass, for coculture and monoculture. B) Simulated species composition.